



Thermal dry reforming of methane over La_2O_3 co-supported $\text{Ni}/\text{MgAl}_2\text{O}_4$ catalyst for hydrogen-rich syngas production

Asif Hussain Khoja¹ · Mustafa Anwar¹ · Sehar Shakir¹ · Muhammad Taqi Mehran² · Arslan Mazhar¹ · Adeel Javed¹ · Nor Aishah Saidina Amin³

Received: 27 March 2020 / Accepted: 6 May 2020 / Published online: 22 May 2020
© Springer Nature B.V. 2020

Abstract

The excess emission of greenhouse gases (GHGs) such as CO_2 and CH_4 is posing an acute threat to the environment, and efficient ways are being sought to utilize GHGs to produce syngas (H_2 , CO) and lighter hydrocarbons (HCs). In this study, the dry reforming of methane (DRM) has been carried out at 700°C using La_2O_3 co-supported $\text{Ni}/\text{MgAl}_2\text{O}_4$ nano-catalyst in a fixed bed thermal reactor. The catalyst is characterized using various techniques such as XRD, FESEM, EDX-mapping, CO_2 -TPD, H_2 -TPR and TGA. The modified MgAl_2O_4 shows the flake type structure after the addition of La_2O_3 . The TPR and TPD analysis shows the highly dispersed metal and strong basic nature of the catalyst consequently enhances the conversion of CO_2 and CH_4 . The highest conversion for CH_4 is 87.3% while CO_2 conversion is nearly 89.5% in 20 h of operation time. The selectivity of H_2 and CO approached 50% making the H_2/CO ratio above unity. In the longer time-on-stream (TOS) test, the catalyst shows elevated potential for longer runs showcasing better catalytic activity. The stability of the catalyst is indicated via a proposed reaction mechanism for DRM in operating conditions. Moreover, TGA indicates the lower weight loss of spent catalyst which ascribed the lower formation of carbon during TOS 20 h.

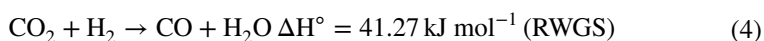
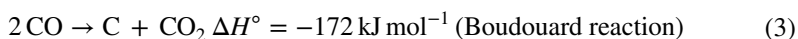
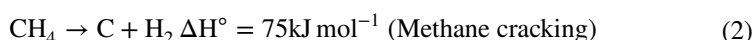
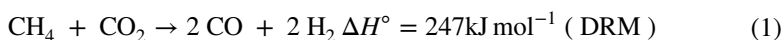
Keywords Dry reforming of methane · thermal reactor · MgAl_2O_4 · H_2 production · syngas

✉ Asif Hussain Khoja
asif@uspcase.nust.edu.pk

Extended author information available on the last page of the article

Introduction

Dry reforming of methane (DRM) (Eq. 1) is an important technique which has been used to convert the greenhouse gases such as CO₂ and CH₄ to syngas (H₂, CO) and lighter hydrocarbons (C₂-C₃) [1]. The syngas can be used as feedstock for the well-known Fischer–Tropsch (FT) synthesis process in gas-to-liquid fuel technology [2]. The CH₄ and CO₂ have been successfully converted into fuels via DRM [3], however, the carbon deposition is a major concern identified in the recent studies [4, 5]. Mainly, the carbon is formed via two famous reactions which are methane cracking (Eq. 2) and Boudouard reaction (Eq. 3) [6]. Another issue is the H₂/CO ratio, which is usually less than unity due to the reverse water gas shift reaction (RWGS) (Eq. 4) [7, 8].



The aim of developing an efficient and stable catalyst is to improve the conversion efficiency, stability and H₂/CO ratio with lower carbon formation [9]. Various catalyst systems were employed to improve the conversion efficiency. The Ni-based catalyst with various supports such as Al₂O₃ [10], MgAl₂O₄ [11], SiO₂ [12], Mesoporous silica molecular sieves (MCM) [13], MgO [14], zeolites [15] and ZrO₂ [16] were reported for DRM [17]. Furthermore, co-supported catalysts were also extensively studied with multiple objectives such as CO₂ adsorption and metal dispersion [14, 18]. The noble metals demonstrate high catalytic activity as well as inhibit the coke formation reported in the literature. However, the high cost makes them less suitable for the commercialization of the DRM process, extensively compiled by Pakhare & Spivey [19].

The Ni-based catalysts need further improvements to make them more viable for the DRM as the carbon growth on Ni sites is the most common issue with the single-supported catalyst. Recently, the co-support system with Ni as active metal is seeking remarkable attention such as Al₂O₃-MgO [20]. To achieve the communal effect of both Al and Mg, the Ni/MgAl₂O₄ spinel has been synthesized for DRM, and it resulted in a stable and enhanced performance than Ni/Al₂O₃. However, issues such as carbon formation and H₂/CO ratio were not resolved [21, 22]. The catalyst performance in the DRM also depends on the physicochemical properties of the material. The physicochemical properties of catalyst can be modified by the preparation techniques and by introducing a co-support which will improve the basicity and metal dispersion on the catalyst support [23–25]. The basic nature of the catalyst is also important for carbon deposition and deactivation of the catalytic performance [26, 27]. Ni interface with MgAl₂O₄ is improved by the communal effect of MgAl₂O₄

and La₂O₃ as mixed matrix support [28]. In thermo-catalytic DRM, the combined effect of La₂O₃ and MgAl₂O₄ catalyst is barely reported [29].

Herein, we investigate the Ni/La-Mg catalyst for high-temperature DRM to analyse the catalytic activity, products distribution and stability during the long-term continuous operation. We prepared the mixed-matrix support nano-catalyst of 10 wt.% Ni/La₂O₃-MgAl₂O₄ and tested for DRM in a fixed bed thermal reactor. The catalyst material was characterized by X-ray diffraction (XRD), field emission electron microscopy (FESEM), H₂ temperature-programmed reduction (H₂-TPR), CO₂ temperature-programmed desorption (CO₂-TPD), N₂ adsorption-desorption (BET) EDX-mapping and TGA. Finally, a probable reaction mechanism was proposed based on product distribution.

Materials and methods

Material synthesis and characterization

MgAl₂O₄ and La₂O₃ spinel was prepared by modifying the co-precipitation method followed by hydrothermal process reported elsewhere [30]. For MgAl₂O₄ the respective nitrate salts were added to ammonia solution with a ratio of 2:1 (Al: Mg). The required quantities of citric acid and dimethylformamide (DMF) were added to improve the metal dispersion and better crystal growth. The solution was kept at 160 °C for 24 h in an autoclave for the hydrothermal process. The slurry was then washed several times using ethanol and DI water, and the samples were dried in an oven. The same method is repeated for the synthesis of La₂O₃. For co-support, MgAl₂O₄ and La₂O₃ were taken as 4:1 (wt. ratio) as co-support and prepared by microemulsion technique [31]. The 10% wt. Ni as the active metal was impregnated by the modified incipient wetness impregnation method [32]. The catalyst was then calcined at 700 °C for 3 h in a muffle furnace. The material was characterized by XRD, FESEM, H₂-TPR, CO₂-TPD, EDX-mapping, BET and TGA. The characterization methods and equipment details were reported elsewhere [32]. The crystallography and morphology of the catalyst were analysed by XRD, FESEM and BET. The crystallite size was calculated using the Scherrer equation [32, 33]. The metal-support interaction and basicity of the materials were analysed by TPR and TPD, and TGA was used to explain the thermal stability of the synthesized material.

Experimental setup and calculations

The experimental setup for the fixed-bed thermal reactor is presented in Fig. 1. Briefly, the feed gases CH₄ (99.99%) and CO₂ (99.99%) controlled by a mass flow controller (ALICAT) were provided to the fixed bed reactor. The fixed-bed reactor consists of a vertical furnace (Carbolite UK) integrated with a thermocouple. The catalyst is loaded in alumina tube (10 mm inner diameter) with the help of quartz wool. A condenser and silica-bed are used to separate the liquid and gaseous products, respectively, before sending the syngas to the gas analysis systems. The products gases were analysed using

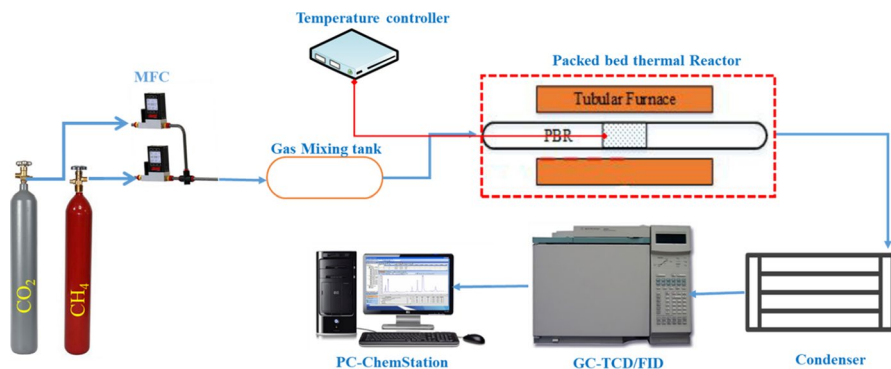


Fig. 1 Experimental setup for thermal catalytic dry reforming of methane

an online gas chromatograph (GC) (Agilent 6890 N) equipped with a thermal conductivity detector (TCD) and flame ionization detector (FID) [29].

The catalytic activity tests were conducted to analyse the performance of the DRM catalyst in a fixed-bed thermal reactor. The reactant conversion (X) and selectivity (S) were calculated according to Eqs. (5–9). When n represents the number of moles of the individual species. The experiments were repeated twice to determine the relative error.

$$\text{CH}_4 \text{ conversion } (X_{\text{CH}_4})\% = \left[\frac{(n_{\text{CH}_4})_{\text{converted}}}{(n_{\text{CH}_4})_{\text{feed}}} \times 100 \right] \quad (5)$$

$$\text{CO}_2 \text{ conversion } (X_{\text{CO}_2})\% = \left[\frac{(n_{\text{CO}_2})_{\text{converted}}}{(n_{\text{CO}_2})_{\text{feed}}} \times 100 \right] \quad (6)$$

$$\text{CO selectivity } (S_{\text{CO}})\% = \left[\frac{(n_{\text{CO}})_{\text{produced}}}{(n_{\text{CH}_4} + n_{\text{CO}_2})_{\text{converted}}} \times 100 \right] \quad (7)$$

$$\text{H}_2 \text{ selectivity } (S_{\text{H}_2})\% = \left[\frac{(n_{\text{H}_2})_{\text{produced}}}{(2 \times n_{\text{CH}_4})_{\text{converted}}} \times 100 \right] \quad (8)$$

$$\text{C}_2\text{H}_6 \text{ selectivity } (S_{\text{C}_2\text{H}_6})\% = \left[\frac{(2 \times n_{\text{C}_2\text{H}_6})_{\text{produced}}}{(n_{\text{CH}_4} + n_{\text{CO}_2})_{\text{converted}}} \times 100 \right] \quad (9)$$

Results and discussion

Physicochemical properties of the material

The crystallographic structure of the prepared catalysts was analysed by X-ray diffraction (XRD) as shown in Fig. 2a. The X-ray diffraction peaks for MgAl₂O₄

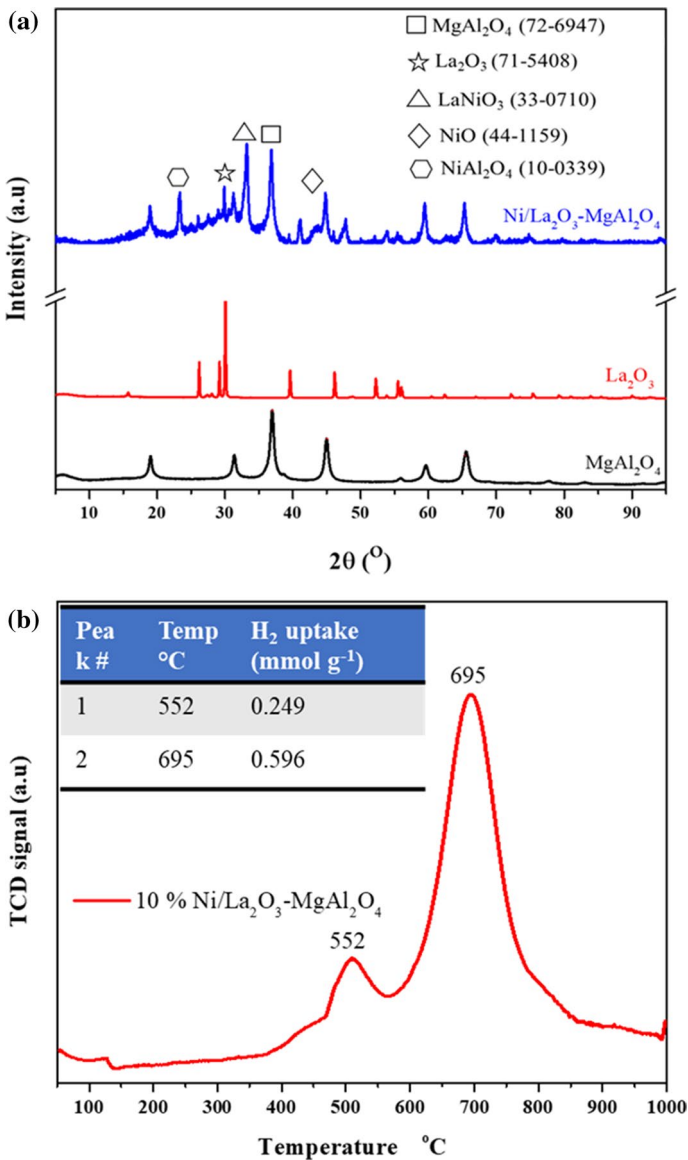


Fig. 2 a XRD of the prepared samples b H₂-TPR with inset H₂ uptake profile and

(PDF#72–6947) were analysed, and the cubical phase (hkl; 311) was confirmed at 38.5° with a space group of 227: Fd3m [24, 34]. The average crystallite size for MgAl_2O_4 was 10.5 nm. Similarly, La_2O_3 (71–5408) was detected in XRD analysis with a major peak at 30.3° (hkl;011) with an average crystallite size of 9.7 nm [35]. The NiO (PDF#44–1159) with major phase (101) was confirmed at 37.5° having an average crystallite size of 10.0 nm [32]. The major peak of NiAl_2O_4 (PDF #10–0339) was detected at 37.09° (311) with a crystallite size of 14.3 nm [36] and LaNiO_3 peak (PDF #33–0710) at 23.08° (100) while the crystallite size is 13.8 [37] with rhombohedral structure.

The reduction behaviour of the developed DRM catalyst was analysed using H_2 -TPR technique depicted in Fig. 2b for the La_2O_3 co-supported Ni/ MgAl_2O_4 calcined at 700°C . The TPR shows the first major peak at 552°C with the H_2 -uptake of $249.3\ \mu\text{mol g}^{-1}$ while the second major peak was detected at 695°C showing H_2 -uptake of $596.6\ \mu\text{mol g}^{-1}$. The total H_2 -uptake of $\sim 850\ \mu\text{mol g}^{-1}$ which shows the 91% degree of reduction [38]. The higher H_2 uptake at elevated temperature shows the good interaction of Ni/ La_2O_3 - MgAl_2O_4 . From the intense TPR peak at 695°C , it is evident that NiO has been reduced into Ni [39].

The basicity of MgAl_2O_4 and Ni/ La_2O_3 - MgAl_2O_4 is investigated using CO_2 -TPD and presented in Fig. 3 and Table 1. Three different peaks present at various regions from weak to strong basic nature of the prepared catalyst. The first two peaks for MgAl_2O_4 at 87°C and 291°C with CO_2 uptake of $347\ \mu\text{mol g}^{-1}$ and $122\ \mu\text{mol g}^{-1}$, respectively, and indicating the weak basic sites [11]. While for Ni/ La_2O_3 - MgAl_2O_4 sample, the first two peaks were detected at 95°C and 361°C with CO_2 uptake of $206\ \mu\text{mol g}^{-1}$ and $110\ \mu\text{mol g}^{-1}$, ascribed to the weak and medium basic sites, respectively. The distant peak shift from weak region to the medium is due to the addition of La_2O_3 . The strong basic sites for MgAl_2O_4 were detected at 542°C

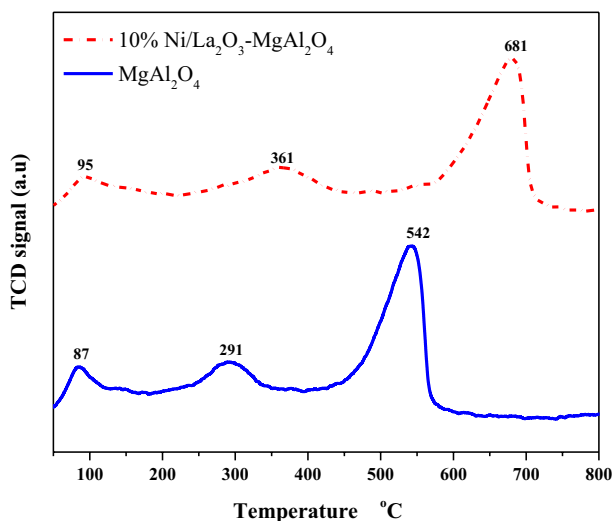


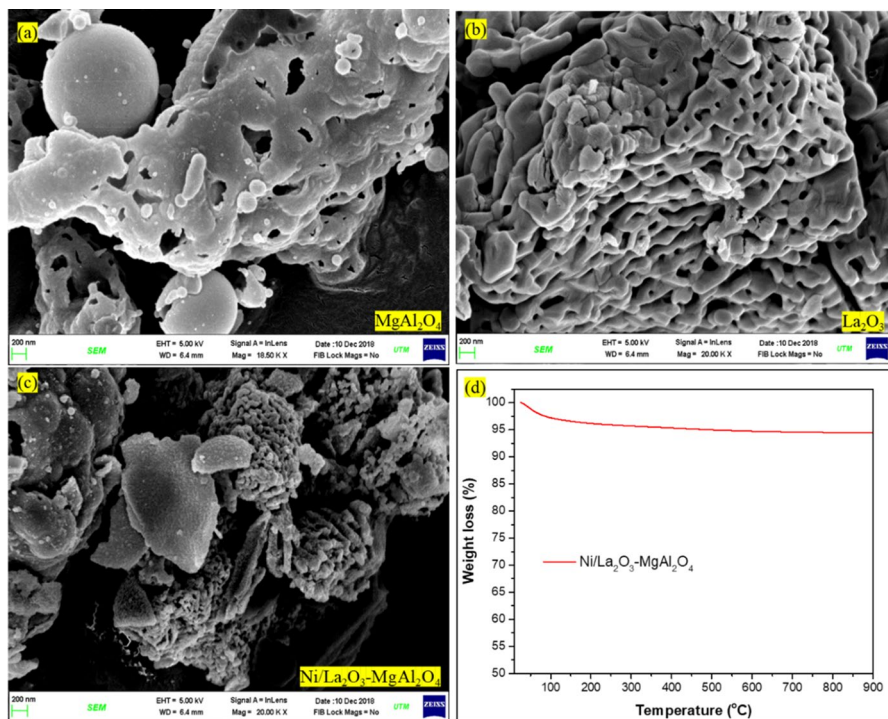
Fig. 3 CO_2 TPD analysis of La_2O_3 co-supported Ni/ MgAl_2O_4 and MgAl_2O_4 with inset CO_2 uptakes

Table 1 CO₂ uptake for MgAl₂O₄ and 10% Ni/La₂O₃-MgAl₂O₄

Peak #	Sample	Temperature (°C)	CO ₂ uptake (μmol g ⁻¹)
1	MgAl ₂ O ₄	80	347
	10% Ni/La ₂ O ₃ -MgAl ₂ O ₄	85	206
2	MgAl ₂ O ₄	291	121
	10% Ni/La ₂ O ₃ -MgAl ₂ O ₄	301	110
3	MgAl ₂ O ₄	542	462
	10% Ni/La ₂ O ₃ -MgAl ₂ O ₄	681	683

having the CO₂ uptake of 463 μmol g⁻¹ [11]. In contrast, for Ni/La₂O₃-MgAl₂O₄ sample, the strong basic sites were present at 681 °C with the CO₂ uptake of 683 μmol g⁻¹. The higher CO₂ uptake at the elevated temperature depicted the strong basic nature of the catalyst which is suitable for the DRM process and it is expected to exhibit better coke resistance during the long-term TOS tests [40].

The morphology of the prepared DRM catalysts was analysed by FESEM and depicted in Fig. 4. The MgAl₂O₄ sample shows agglomerated porous structure presented in Fig. 4a and La₂O₃ shows a uniform web-like structure is evident in the

**Fig. 4** FESEM micrographs of **a** MgAl₂O₄ **b** La₂O₃ **c** La₂O₃ co-supported Ni/MgAl₂O₄ **d** TGA of La₂O₃ co-supported Ni/MgAl₂O₄

modified preparation method using DMF as a surfactant which also assists in the uniform crystal growth (Fig. 4b). La_2O_3 co-supported $\text{Ni}/\text{MgAl}_2\text{O}_4$ sample resulted in a nanoflake-type structure depicted in Fig. 4c. The irregular structure of MgAl_2O_4 is modified by web-like La_2O_3 infusing with the Ni particles. Furthermore, the thermal stability of the La_2O_3 co-supported $\text{Ni}/\text{MgAl}_2\text{O}_4$ presented in Fig. 4d. The total weight loss is less than 3.5% in the temperature range of 125 °C is ascribed to the removal of moisture [41].

The N_2 adsorption–desorption isotherms, surface area (S_{BET}), average pore volume (V_{pore}) and average pore radius is presented in Fig. 5. The samples exhibited type IV isotherm confirming the formation of mesoporous structure material for all the synthesized samples. The surface area of MgAl_2O_4 and La_2O_3 was $102 \text{ m}^2 \text{ g}^{-1}$ and $41.3 \text{ m}^2 \text{ g}^{-1}$, respectively. While the addition of Ni into La_2O_3 - MgAl_2O_4 reduces the surface area to $90 \text{ m}^2 \text{ g}^{-1}$. It is ascribed to the infusion of Ni particle on the surface of the catalyst support. The average pore radius of the MgAl_2O_4 , La_2O_3 and $\text{Ni}/\text{La}_2\text{O}_3$ - MgAl_2O_4 is 8.6 nm, 5.7 nm and 8.1 nm, respectively.

Catalyst performance analysis

The DRM activity test has been carried out using the developed catalyst shown in Fig. 6. At first, the DRM was carried out without a catalyst which shows very low catalytic activity. The conversion of CH_4 and CO_2 is just below 10% at 700 °C. The selectivity of H_2 and CO is found to be less than 6%. In contrast, adding MgAl_2O_4 catalyst in the fixed bed, the increment in the conversion and selectivity of the product is observed. The conversion of CH_4 and CO_2 is 35% and 32%, respectively. The selectivity H_2 , CO and C_2H_6 is less than 12%, 15% and 3.5% respectively. The Ni impregnation in MgAl_2O_4 further improves the catalytic activity with the increase

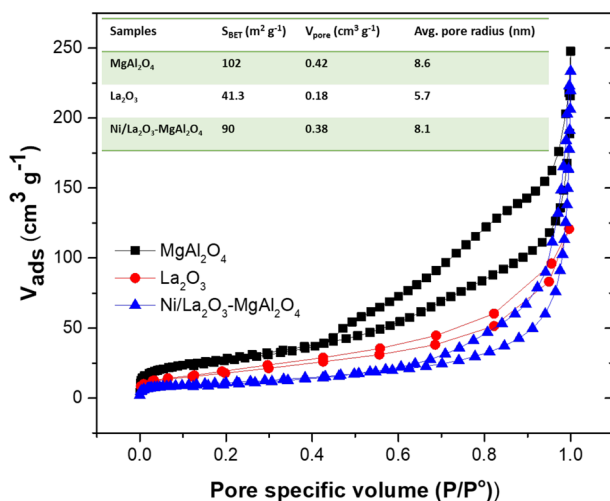


Fig. 5 N_2 adsorption–desorption of prepared samples with inset specific surface area (S_{BET}) $\text{m}^2 \text{ g}^{-1}$, average pore volume (V_{pore}) $\text{cm}^3 \text{ g}^{-1}$ and average pore radius (nm)

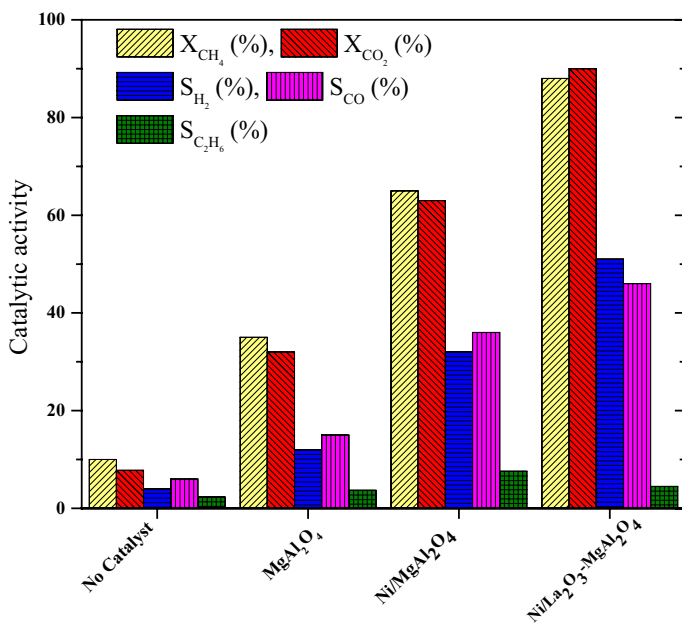


Fig. 6 Catalysts performance evaluation: GHSV=1500 h⁻¹, catalyst loading=0.3 g, feed ratio (CO₂/CH₄)=1, reaction temperature=700 °C, reaction time=2 h

in the conversion of CH₄ and CO₂ to 65 and 63%. Ni /MgAl₂O₄ also substantially improves the selectivity of H₂, CO and C₂H₆ to 32%, 35% and 7.5% as depicted in Fig. 6. Whereas, incorporating 20% La₂O₃ as co-support into 10%Ni/MgAl₂O₄ enhances the conversion of CH₄ and CO₂ to 87.3% and 89.5%, respectively. The selectivity of the H₂ improves from 32 to 51% for the composite La₂O₃ co-supported Ni/MgAl₂O₄ catalyst. CO selectivity is recorded 46% which is less than the selectivity of H₂. In contrast, C₂H₆ selectivity decrease to 4.5% in the La₂O₃ co-supported Ni/MgAl₂O₄. This might be due to the higher yield and inhibition of methyl radical recombination [23].

The overall catalytic activity of the reported samples is in such order: MgAl₂O₄<Ni/MgAl₂O₄<La₂O₃ co-supported Ni/MgAl₂O₄. The non-co-supported catalyst activity is lower than that of Co-supported catalyst, which ascribes the occurrence of reverse water gas shift (RWGS) reaction is limited [23]. The La₂O₃ co-supported catalyst resists the progress of RWGS and H₂ selectivity is improved. Furthermore, the possible formation of La₂O₂CO₃ inhibit the carbon formation and improves the catalyst activity [23]. The improvement in the CH₄ conversion is due to the good formation of active sites as depicted in H₂-TPR results. The bulk formation of active sites activates CH₄ and resist the C_xH_x recombination by a further breakdown.

The comparison with the literature is drawn in Table 2 for the reference. As we can see that the majority of the reports shows the H₂/CO ratio below 1.0 except for Ni/h-BNNs catalyst reported by [42]. The higher H₂/CO ratio depicts the CH₄ decomposition or Boudouard reaction. These reactions usually occur on Ni active

Table 2 Literature comparison with current study thermal DRM on La_2O_3 co-supported $\text{Ni}/\text{MgAl}_2\text{O}_4$ catalyst

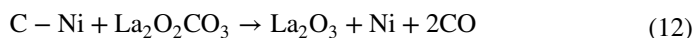
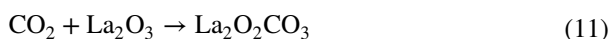
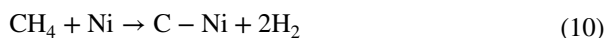
Catalyst	Parameters	X_{CH_4} (%)	X_{CO_2} (%)	H_2/CO ratio	Ref
$\text{Pv}/\text{CePr}/\text{Al}_2\text{O}_3$	$\text{CH}_4/\text{CO}_2 = 1$, 100 ml min^{-1}	69	77	0.9	[43]
$\text{Ni}/\text{Sn}0.02/\text{Al}$	100 ml min^{-1} , $\text{CH}_4/\text{CO}_2 = 1$, WHSV, $60,000 \text{ ml g}^{-1}\text{cat h}^{-1}$	42	78	0.9	[44]
Ni/Al	100 ml min^{-1} , $\text{CH}_4/\text{CO}_2 = 1$, WHSV, $60,000 \text{ ml g}^{-1}\text{cat h}^{-1}$ $700 \text{ }^\circ\text{C}$	49	76	0.8	[44]
$\text{Ni}/\text{h-BNNs}$	100 ml min^{-1} , $\text{CH}_4/\text{CO}_2 = 1$, WHSV, $35,000 \text{ ml g}^{-1}\text{cat h}^{-1}$	90	70	1.05	[42]
$\text{Ni}/\text{La}_2\text{O}_3\text{-LOC}$	$\text{CH}_4/\text{CO}_2 = 1$, WHSV = $60,000 \text{ mL h}^{-1} \text{ gcat}^{-1}$, $700 \text{ }^\circ\text{C}$	78	81	0.89	[23]
$\text{Ni}_{0.07}\text{Mg}_{0.93}\text{O-R}$	$\text{CH}_4/\text{CO}_2 = 1$, WHSV = $86,000 \text{ mL h}^{-1} \text{ gcat}^{-1}$, $800 \text{ }^\circ\text{C}$	82	88	0.9	[45]
$\text{Ni}/\text{La}_2\text{O}_3\text{-Al}_2\text{O}_3$	$\text{CH}_4/\text{CO}_2 = 1$, GHWSV = 60 mL gcat^{-1} , $700 \text{ }^\circ\text{C}$	82.4	77.3	0.95	[24]
$\text{Ni}/\text{La}_2\text{O}_3\text{-MgAl}_2\text{O}_4$	$\text{CH}_4/\text{CO}_2 = 1$, GHWSV = $15,000 \text{ h}^{-1}$, $700 \text{ }^\circ\text{C}$	87.3	89.5	1.1	This work

sites and block them, however, if α -C is formed, it can be easily gasified or reacts with La₂O₃ to form La₂O₂CO₃ [23, 42]. The addition of La₂O₃ also assists the chemisorption of CO₂ and regeneration of active metal and La₂O₃ along with major support MgAl₂O₄ [23, 24].

Catalyst stability and reaction mechanism

The catalyst stability is one of the most important parameters after the fundamental catalytic performance. Herein, the La₂O₃ co-supported Ni/MgAl₂O₄ was tested for 20 h of time on stream (TOS) test keeping the process parameters constant. The conversion of CH₄ is shown in Fig. 7a, a stable trend having only 03% reduction in 20 h of TOS observed. Similarly, CO₂ also shows the same trend in the same TOS and experimental conditions. The stable conversion in the reported TOS for both reactants is encouraging for the reported catalyst. The selectivity of the H₂ and CO partly declined during the 20 h TOS presented in Fig. 7b. The selectivity of the C₂H₆ is slightly higher in the 20 h TOS. Figure 8 shows that the H₂/CO ratio is above unity during the 20 h TOS indicating the low carbon formation over the catalyst and enhanced stability.

The conversion stability of the developed catalyst is associated with better metal-support interaction (MSI high active sites and high basicity due to the addition of La₂O₃). It also supports methane activation as well as CO₂ adsorption due to its basic nature [46]. The CH₄ activation is due to the Ni and formed Ni-C and 2H₂ (Eq. 10). The formation of La₂O₂CO₃ intermediate carbonate during the adsorption of CO₂ (Eq. 11) and after reaction with C-Ni to regenerate the La₂O₃, Ni and CO resist the carbon deposition on the catalyst surface (Eq. 12) [47]. The schematic representation of the reaction mechanism is proposed in Fig. 9.



Characterization of the spent catalyst

After 20 h of TOS, the spent catalyst has been characterized by EDX mapping and TGA. Figure 10a presented elemental mapping shows the formation of carbon over the surface of the catalyst. The mapping indicates the formation of carbon is not in the bulk form (Fig. 10b). The inset FESEM shows the formation of carbon nanofibres on the surface of the spent catalyst. The carbon nanofibres can easily reduce in the gasification process and formed CO or CO₂.

The TGA profile of the spent La₂O₃ co-supported Ni/MgAl₂O₄ after 20 h of TOS shows the total weight loss of 9–10%, which confirms the formation of a lower amount

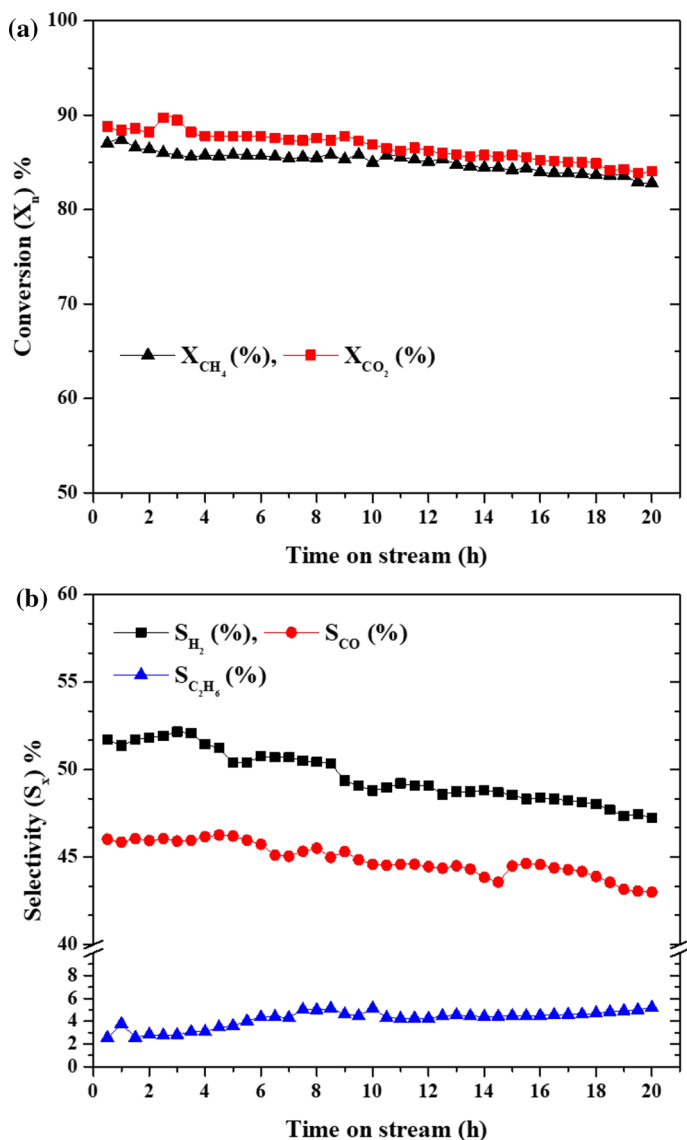


Fig. 7 Effect of time on stream **a** conversion of reactants (X_n) **b** H_2 , CO and C_2H_6 selectivity (S_x) over La_2O_3 co-supported $Ni/MgAl_2O_4$; GHSV = 1500 h^{-1} , catalyst loading = 0.3 g, feed ratio (CO_2/CH_4) = 1, reaction temperature = $700\text{ }^\circ\text{C}$

of carbon. The moisture and volatile matter removal are at $200\text{ }^\circ\text{C}$ [11, 48] presented in Fig. 11. The weight loss in between 200 – $500\text{ }^\circ\text{C}$ is associated with the fibrous carbon which is referred as β -carbon, as well as the decomposition of La-hydroxide intermediate phase which is usually formed under the moist conditions due to RWGS [29]. The total of 3% weight loss between 500 – $900\text{ }^\circ\text{C}$ (Column III-IV) which confirm the low

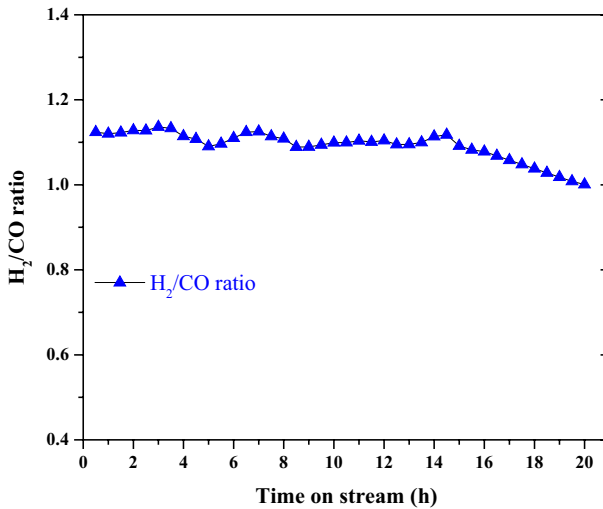


Fig. 8 Time on stream vs H₂/CO ratio over La₂O₃ co-supported Ni/MgAl₂O₄; GHSV = 1500 h⁻¹, catalyst loading = 0.3 g, feed ratio (CO₂/CH₄) = 1, reaction temperature = 700 °C

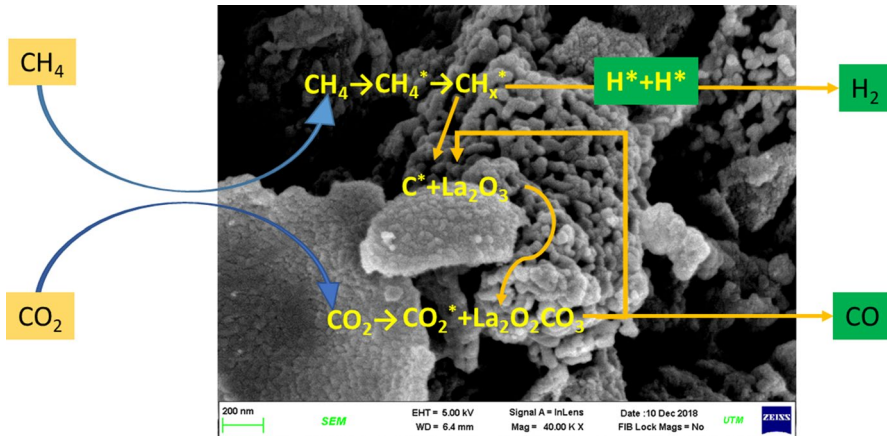


Fig. 9 Proposed reaction mechanism for La₂O₃ co-supported Ni/MgAl₂O₄ based DRM

formation of carbon after 20 h TOS. This reduction is also ascribed to the dissociation of La₂O₂CO₃ [49]. The carbon formed above 700 °C is ascribed to filamentous carbon (γ-C).

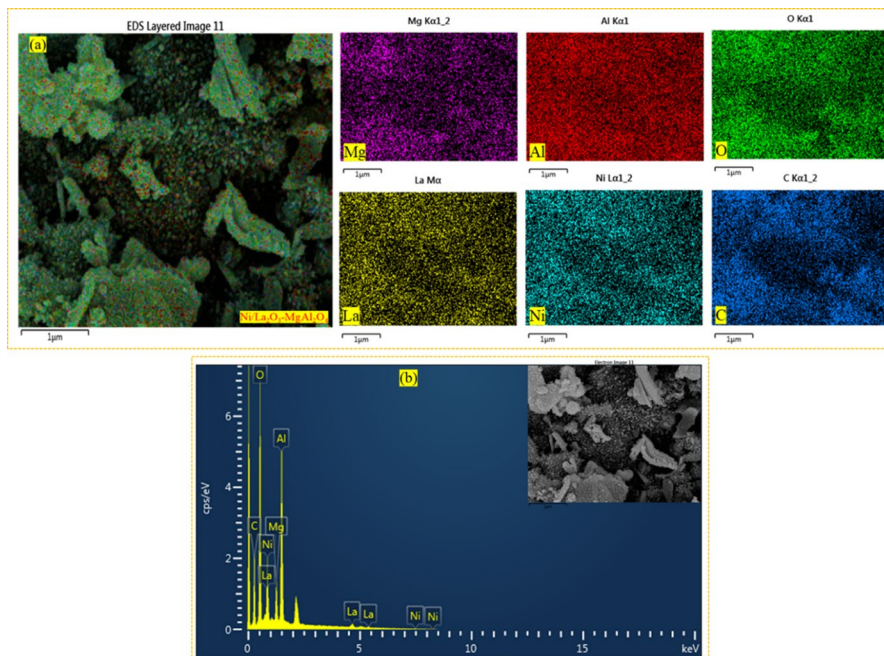


Fig. 10 a EDX mapping of spent catalyst b EDX elemental analysis with inset FESEM

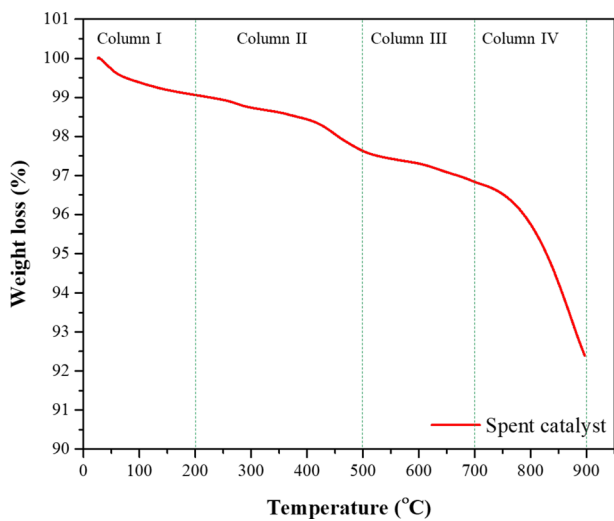


Fig. 11 TGA profile of spent La_2O_3 co-supported $\text{Ni/MgAl}_2\text{O}_4$ after 20 h TOS

Conclusions

The synthesized La₂O₃ co-supported Ni/MgAl₂O₄ has been characterized using various techniques and employed for the DRM in thermal fixed bed reactor. The catalyst shows enhanced performance and higher H₂/CO ratio, much suitable feedstock for downstream chemicals. The enhanced performance is ascribed to the suitable physicochemical properties of a catalyst such as metal-support interaction and the strong basic nature with well-structured morphology. While testing for longer runs, the catalyst shows stability for 20 h with less than 3% declined in the DRM activity and TGA of spent catalyst confirms the lower formation of carbon. This stability suggests the potential of the upgradation of the developed catalyst for the DRM process for industrial-scale production of syngas.

Authors Contribution

Asif Hussain Khoja and Nor Aishah Saidina Amin develop the conceptualization of the work and drafted the manuscript. Arslan Mazhar assisted in material synthesis and in conducting the experiments. Mustafa Anwar and Sehar Shakir workout the material characterization analysis. Muhammad Taqi Mehran assisting in the result analysis of GC, drafting and revising the manuscript.

Acknowledgements The authors would like to extend their deepest appreciation to the Universiti Teknologi Malaysia for the financial support of this research under RUG (Research University Grant, Vot13H35) and FRGS-MRSA grant.


References

1. J.A. Frankel, *Greenhouse Gas Emissions* (Brookings Institution, Washington, D.C, 1999)
2. A. Rafiee, K. Rajab Khalilpour, D. Milani, M. Panahi, J. Environ. Chem. Eng. 6(5), (2018)
3. R. Dębek, K. Zubek, M. Motak, P. Da Costa, T. Grzybek, Res. Chem. Intermed. 41(12), (2015)
4. A.H. Khoja, M. Tahir, N.A.S. Amin, Energy Convers. Manag. 183, (2019)
5. M.A. Gerber, *Review of Novel Catalysts for Biomass Tar Cracking and Methane Reforming* (Pacific Northwest National Laboratory Richland, WA, USA, 2007)
6. Y.H. Hu, E. Ruckenstein, Adv. Catal. 48(49), (2004)
7. B. Abdullah, N.A.A. Ghani, D.V.N. Vo, J. Clean. Prod. 162, (2017)
8. E. Horvath, K. Baan, E. Varga, A. Oszko, A. Vago, M. Toro, A. Erdohelyi, Catal. Today 281, (2017)
9. M. Usman, W.M.A.W. Daud, H.F. Abbas, Renew. Sustain. Energy Rev. 45, (2015)
10. K. Selvarajah, N.H.H. Phuc, B. Abdullah, F. Alenazey, D.-V.N. Vo, Res. Chem. Intermed. 42(1), (2016)
11. I.H. Son, S. Kwon, J.H. Park, S.J. Lee, Nano Energy 19, Supplement C (2016)
12. S. Tomiyama, R. Takahashi, S. Sato, T. Sodesawa, S. Yoshida, Appl. Catal. A Gen. 241(1–2), (2003)
13. H. Arbag, S. Yasyerli, N. Yasyerli, G. Dogu, Int. J. Hydrog. Energy 35(6), (2010)
14. Y.J.O. Asencios, E.M. Assaf, Fuel Process. Technol. 106, (2013)
15. P. Frontera, A. Aloise, A. Macario, F. Crea, P.L. Antonucci, G. Giordano, J.B. Nagy, Res. Chem. Intermed. 37(2), (2011)
16. N. Rahemi, M. Haghghi, A.A. Babaluo, M.F. Jafari, P. Estifae, J. Ind. Eng. Chem. 19(5), (2013)
17. V. Sadykov, V. Rogov, E. Ermakova, D. Arendarsky, N. Mezentseva, G. Alikina, N. Sazonova, A. Bobin, S. Pavlova, Y. Schuurman C. Mirodatos, Thermochem. Acta 567, (2013)

18. S.H. Zeng, L. Zhang, X.H. Zhang, Y. Wang, H. Pan, H.Q. Su, *Int. J. Hydrog. Energy* 37(13), (2012)
19. D. Pakhare, J. Spivey, *Chem. Soc. Rev.* 43(22), (2014)
20. L. Zhang, Q. Zhang, Y. Liu, Y. Zhang, *Appl. Surf. Sci.* 389, Supplement C (2016)
21. S. Dash, R.K. Sahoo, A. Das, S. Bajpai, D. Debasish, S.K. Singh, *J. Alloys Compd.* 726, Supplement C (2017)
22. H.-J. Kim, E.-H. Yang, Y.S. Noh, G.H. Hong, J.I. Park, S.A. Shin, K.-Y. Lee, D.J. Moon, *Res. Chem. Intermed.* 44(2), (2017)
23. X.Y. Li, D. Li, H. Tian, L. Zeng, Z.J. Zhao, J.L. Gong, *Appl. Catal. B-Environ.* 202, (2017)
24. A.S. Al-Fatesh, M.A. Naem, A.H. Fakeeha, A.E. Abasaheed, *Chin. J. Chem. Eng.* 22(1), (2014)
25. M.A. Uzair, A. Waqas, A.H. Khoja, N. Ahmed, *Energy Source Part A* 38(24), (2016)
26. A.H. Khoja, M. Tahir, N.A.S. Amin, A. Javed, M.T. Mehran, *Int. J. Hydrog. Energy* 45(22), (2020)
27. R. Pereñiguez, V.M. Gonzalez-delaCruz, A. Caballero, J.P. Holgado, *Appl. Catal. B: Environ.* 123, (2012)
28. D.X. Li, P. Pirouz, A.H. Heuer, S. Yadavalli, C.P. Flynn, *Philos. Mag. A* 65(2), (1992)
29. A.H. Khoja, M. Tahir, N.A.S. Amin, *Energy Convers. Manag.* 144, (2017)
30. A. Samad, K.Y. Lau, I.A. Khan, A.H. Khoja, M.M. Jaffar, M. Tahir, *J. Phys. Chem. Solids* 120, (2018)
31. M. Usman, W.M.A.W. Daud, *RSC Adv.* 6(44), (2016)
32. A.H. Khoja, M. Tahir, N.A.S. Amin, *Fuel Process. Technol.* 178, (2018)
33. A.H. Khoja, M. Tahir, N.A. Saidina Amin, *Energy Fuels* 33(11), (2019)
34. S. Sokolov, E.V. Kondratenko, M.M. Pohl, A. Barkschat, U. Rodemerk, *Appl. Catal. B-Environ.* 113, (2012)
35. D. Ağaogulları, İ. Duman, M.L. Öveçoğlu, *Ceramics Int.* 38(8), (2012)
36. N. Sahli, C. Petit, A.C. Roger, A. Kiennemann, S. Libs, M.M. Bettahar, *Catal. Today* 113(3), (2006)
37. X. Song, X. Dong, S. Yin, M. Wang, M. Li, H. Wang, *Appl. Catal. A Gen.* 526, (2016)
38. A. Bordoloi, S. Das, R. Goyal, R.K. Singha, C.R. Pendem, S.K.L. Narayan, R. Bal, V.V.D.N. Prasad, N.N. Botcha, M. Kumar, (Google Patents, 2017)
39. J. Shen, A.A.C. Reule, N. Semagina, *Int. J. Hydrog. Energy* 44(10), (2019)
40. S. Das, M. Sengupta, J. Patel, A. Bordoloi, *Appl. Catal. a-Gen.* 545, Supplement C (2017)
41. J. Guo, H. Lou, H. Zhao, X. Zheng, *React. Kinet. Catal. Lett.* 84(1), (2005)
42. Y. Cao, P. Maitarad, M. Gao, T. Taketsugu, H.R. Li, T.T. Yan, L.Y. Shi, D.S. Zhang, *Appl. Catal. B-Environ.* 238, (2018)
43. R.O. da Fonseca, R.C. Rabelo-Neto, R.C.C. Simões, L.V. Mattos, F.B. Noronha, *Int. J. Hydrog. Energy* 45(8), (2020)
44. U. Guharoy, E. Le Sache, Q. Cai, T.R. Reina, S. Gu, *J. CO₂ Util.* 27, (2018)
45. T. Zhang, Z. Liu, Y.-A. Zhu, Z. Liu, Z. Sui, K. Zhu, X. Zhou, *Appl. Catal. B: Environ.* 264, (2020)
46. L. Zhang, X. Wang, C. Chen, X. Zou, X. Shang, W. Ding, X. Lu, *RSC Adv.* 7(53), (2017)
47. J.K. Xu, W. Zhou, J.H. Wang, Z.J. Li, J.X. Ma, *Chin. J. Catal.* 30(11), (2009)
48. C.C. Chong, Y.W. Cheng, H.D. Setiabudi, N. Ainirazali, D.-V.N. Vo, B. Abdullah, *Int. J. Hydrog. Energy* 45(15), (2020)
49. E.P. Komarala, I. Komissarov, B.A. Rosen, *Catalysts* 10(1), (2019)

Publisher's Note Springer Nature remains neutral with regard to jurisdictional claims in published maps and institutional affiliations.

Affiliations

Asif Hussain Khoja¹  · Mustafa Anwar¹ · Sehar Shakir¹ ·
Muhammad Taqi Mehran² · Arslan Mazhar¹ · Adeel Javed¹ ·
Nor Aishah Saidina Amin³

¹ Fossil Fuel Laboratory, Department of Thermal Energy Engineering, U.S.-Pakistan Centre for Advanced Studies in Energy (USPCAS-E), National University of Sciences and Technology (NUST), H-12 Sector, Islamabad 44000, Pakistan

- ² Department of Chemical Engineering, School of Chemical and Materials Engineering (SCME), National University of Sciences and Technology (NUST), H-12 Sector, Islamabad 44000, Pakistan
- ³ Chemical Reaction Engineering Group (CREG), School of Chemical and Energy Engineering, Faculty of Engineering, Universiti Teknologi Malaysia (UTM), 81310 Skudai, Johor Bahru, Malaysia